Advances in Engineering Research, volume 176
The 9th Russian-Chinese Symposium. Coal in the 21st Century: Mining, Intelligent Equipment and Environmental Protection

Monitoring on Ground Movement of Geological Tectonic Region Based on InSAR Time Series Analysis

Shenwen Yu
College of Mining and Safety Engineering
Shandong University of Science and Technology
Qingdao, China
skdkyswc@126.com

Weiping Shi
College of Mining and Safety Engineering
Shandong University of Science and Technology
Qingdao, China
swp1128@163.com

Leyin Hu
Beijng Earthquake Agency
Beijing, China
huleyin@bjseis.gov.cn

Yougui Feng
Shandong Zhengyuan aeronautical Remote Sensing Technology Co., Ltd.
Jinan, China
fengyougui@zyrs.cn

Zhurong Xing
College of Land Resources and surveying Engineering
Shandong Agriculture and Engineering University
Jinan, China
xingzhurong@163.com

***Abstract*--In long-term slow ground deformation monitoring, conventional InSAR technology is affected by factors of temporal decoherence, spatial decoherence and atmospheric effects. In order to overcome these limitations, this paper uses two InSAR time series analysis of permanent scatters and small baseline subset methods to analyze ground deformation caused by fault movement. Based on principles, 34 scenes ENVISAT-ASAR data covered the Dangxiong area were processed in this paper. The results show that, southern fault of Nyenchen Tanglha (northwest margin of Yangbajing-Dangxiong basin) presents a trend of ground uplift. Flat area in the middle of Yangbajing-Dangxiong basin presents a trend of ground subsidence. The front fault of Tanggula Mountain (southeast margin of Yangbajing-Dangxiong basin) presents a trend of ground subsidence. These results were accordance with fault movement in situ. When fault moving, high-level areas were pushed to uplift, while the low-lying areas were squeezed to subsidence. This demonstrates that InSAR time series analysis of permanent scatters and small baseline subset methods are reliable in fault movement monitoring. The fault activity can be analyzed based on monitoring results. This will provide data for earthquake prediction.**

Keywords—InSAR, permanent scatters, small baseline subset, ground movement, geological tectonic region

I. INTRODUCTION

China is located at the intersection of the Circum-Pacific seismic belt and the Eurasian seismic belt, thus earthquakes occur frequently in this intersection. Such as the Mani earthquake in 1997, the Ms8.1 earthquake in Kunlun Mountain in 2001, the Jiashi-Bachu Ms 6.8 earthquake in 2003, the Wenchuan Ms8.0 earthquake and the Dangxiong Ms6.6 earthquake in 2008, etc., brought a great impact on local life and production. The gestation and occurrence of earthquakes are the result of long-term slow movement of earth's crust. Therefore, it is of great significance to monitor the long-term slow deformation of the ground surface for earthquake prediction, especially at faults locations [1]. The difficulty in fault motion monitoring is how to obtain sufficiently and accurately deformation data. High-precision GPS, leveling, seismic stations, etc. all can provide a certain amount of monitoring data, but the cost of manpower and material resources is too high. They are far from meeting the needs of earthquake predictions on both time and space scales [2-5]. InSAR technology is a new ground deformation monitoring technology developed in recent years. It can obtain long-term ground slow deformation information, and its measurement accuracy can reach cm-mm [6] In theory, InSAR technology can obtain large-scale continuously deformation data with cm-mm accuracy. However, in actual operation, it is difficult to achieve mm accuracy due to influence of atmospheric delay, elevation error, vegetation, and random noise.

In order to overcome the limitations in InSAR technology and realize long-term deformation monitoring in a certain area, researchers began to focus on the InSAR time series analysis method based on long time radar image sequence. Based on the idea of interference point target analysis, Ferretti and Prati proposed the permanent scatters (PS) method [7]. In 2001, Berardino and Lanari et al. [8] proposed small baseline subset (SBAS) InSAR technology. PS-InSAR and SBAS-InSAR are two kinds of time series deformation analysis methods, which overcome some of the limitations of traditional InSAR techniques, such as baseline decoherence of temporal and spatial, atmospheric effects, and can obtain ground deformation information in a long time series. In 2010, Joong-Sun et al. [9] processed the ERS-1/2 and ENVISAT-ASAR data covering the southern area of the San Andreas fault zone in the United States based on InSAR time series analysis technology, and obtained the deformation monitoring results in the line of sight in this area. In 2011, Qu et al. [10] obtained the deformation rate of

6-7 mm/a in Haiyuan fault zone by using 21 scenes ENVISAT-ASAR data and PS-InSAR technique. In 2014, Meng et al. [11] used PS-InSAR technology and 14 scenes ENVISAT-ASAR data covering the Ganggu area of the northern margin of the western Qinling Mountains to detect the crustal microdeformation in this area. Casu F. [12] used SBAS to measure the subsidence of Naples Bay in Italy and Los Angeles in the United States. Compared with leveling and GPS data, it is proved that the performance of SBAS method is very superior, and the standard variance of monitored deformation velocity is about 1 mm/year. Liu et al. [13] using the SBAS method to monitor the small and slow deformation of the edge of the mining area, and obtained the spatial distribution of the ground subsidence. Based on ENVISAT-ASAR data, Sun and others [14] used SBAS-InSAR technology to monitor the ground subsidence in Chengdu Plain from 2008 to 2010. Zhou et al. [15] used SBAS-InSAR to obtain ground subsidence information in Beijing area. 18 ENVISAT-ASAR images were used to complete the temporal and spatial analysis of ground subsidence in Beijing area from 2007 to 2010. Li et al. [16] used SBAS-InSAR technique to monitor the seasonal frozen soil deformation in the Qinghai-Tibet Plateau. Based on Jiuzhaigou earthquake (M = 7.0) in the northeast segment of Bayanhar, Zhao et al. [17] derived the coseismic deformation and fault model from InSAR and GPS measurement results. Using regional seismic waveforms and InSAR measurements, Liu et al. [18] determined the focal parameters of the 2016 Menyuan earthquake in northeastern of Qinghai-Tibet Plateau.

Taking Dangxiong region as the study area, in order to obtain ground deformation of this area, PS-InSAR and SBAS-InSAR methods were used in this paper to process the 34 scenes ENVISAT-ASAR data covering the study area from 2003 to 2008. Based on processed data, this paper analyzed the ground movement of study area. Combined with geological technics of study area, the reliability of PS-InSAR and SBAS-InSAR methods has been analyzed in this paper.

II. TECTONIC BACKGROUND OF THE STUDY AREA

Dangxiong region is located in the middle of Lhasa block, with an average elevation of about 5000 m. The highest elevation of the main peak Nyenchen Tanglha is about 7111 m. The famous Yangbajing-Dangxiong basin was located on the east side of Nyenchen Tanglha, This region was influenced by complex geological tectonics and developed the famous Dangxiong-Yangbajing active fault. The Dangxiong-Yangbajing fault is an oblique slip fault with both left-lateral strike-slip and normal-dip slip. It is an important dividing line in geological structure and geomorphology between eastern and western of Tibet. And the Dangxiong-Yangbajing fault is an important seismicity zone and geothermal active zone in central of Tibet[19]. The first wet steam geothermal power station is built in the north of this study area. Topography map in Dangxiong area was shown in Fig. 1.

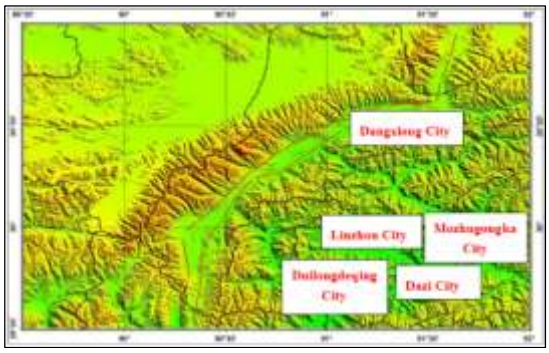

Fig.1. Topography map in Dangxiong area (Faults shown in red lines)

III. PRINCIPLE OF INSAR TIME SERIES ANALYSIS

A. *Principles of PS-InSAR*

This technique uses a two-dimensional linear (or nonlinear) phase regression analysis model to obtain the deformation information from the differential interferometric phase of PS that remains highly coherent over long time intervals.

It is assumed that there are N + 1 SAR images. One image is public main image, the other N images are auxiliary images. The N auxiliary images are registered and interfered with public main image, respectively. And the N interferograms can be expressed as:

$$\phi_{\text{int}} = \phi_{def} + \phi_{topo} + \phi_{atm} + \phi_{flat} + \phi_{noisei} \tag{1}$$

where ϕ_{def} is deformation phase; ϕ_{topo} is topography phase; ϕ_{atm} is atmospheric delay phase; ϕ_{flat} is flat phase; ϕ_{noise} is noise phase.

After differential interference processed with an external DEM, the differential interference phase is:

$$\phi_{\text{diff}} = \phi_{\text{def}} + \phi_{\text{topo}_{\text{error}}} + \phi_{\text{flat}_{\text{error}}} + \phi_{\text{atm}} + \phi_{\text{noise}} \tag{2}$$

where ϕ_{def} is the phase generated by the deformation of ground in periods of two imaging process; $\phi_{\text{topo\_error}}$ is the topographic residual phase caused by an external DEM error; $\phi_{\text{flat\_error}}$ is the residual flat-earth phase caused by satellite orbit errors; $\phi_{\text{flat\_error}}$ is the delayed phase caused by a radar signal passing through an inhomogeneous atmosphere on two imaging times; ϕnoise is noise phase. The first two terms of the formula are the main phase, and the last three terms are residual phases, which are represented by ϕres, then

$$\phi_{\text{diff}} = \phi_{\text{def}} + \phi_{topo_{eror}} + \phi_{\text{res}} \tag{3}$$

Assumed that $\Delta d = v \bullet T$, where v is the deformation rate, then

$$\phi_{\text{def}} = k_1 v \bullet T + k_2 \Delta \text{h}_{\text{error}} + \phi_{res,x,i}$$
$$k_1 = \frac{4\pi}{\lambda}, k_2 = -\frac{4\pi B_{\perp}}{\lambda R \sin\theta} \tag{4}$$

where T is the interval between two imaging times; Δh_{error} is the elevation fuzzy number; k_1, k_2 are coefficients.

From the above formula, it can be seen that phase difference model is a two-dimensional linear phase model. The linear rate of ground deformation, residual DEM error and various noise phases can be obtained by multiple regression analysis.

B. Principles of SBAS

It is assumed that there are N+1 SAR images in the study area, and the acquisition time is in turn as t_0, t_1, …, t_n. According to the temporal and spatial baseline conditions, one of the images is selected as the public main image, and the other N images are as auxiliary images. Thus M interference image pairs are obtained. Assumed that the j interference pair is generated after the interference processing of these two SAR images obtained at moments t_A and t_B, thre inteference phase $\delta\phi_j$ can be expressed as follows,

$$\delta\phi_j = \phi(t_B) - \phi(t_A) \approx \frac{4\pi}{\lambda}\left[d(t_B) - d(t_A)\right] \tag{5}$$

where $d(t_A)$ and $d(t_B)$ are the cumulative deformation information of t_A and t_B relative to the reference time t_0 (assuming $d(t_0)\equiv 0$), and the corresponding phase values are indicated by $\phi(t_A)$ and $\phi(t_B)$.

The vector $\phi_T=[\varphi(t_1),\ldots,\varphi(t_N)]$ are used to denote N phase maps, and vector $\delta\phi_T=[\delta\varphi_1,\ldots\delta\varphi_N]$ denotes M interference phase maps, in which the corresponding main and auxiliary image time series of M interference phase maps are expressed in the following formula,

$$\mathrm{IM}^T = \left[IM_1,\cdots,IM_M\right]; IS^T = \left[IS_1,\cdots,IS_M\right] \tag{6}$$

where *IM* denotes the main image of the interference image pair, and *IS* denotes the auxiliary image of the interference image pair. Assumed that the acquisition time of main image pair precedes the acquisition time auxiliary image pair, then,

$$\delta\phi_j = \phi(t_{ISj}) - \phi(t_{IMj}),\ j = 1,\cdots,M \tag{7}$$

Equations (6)-(7) can be used to define a system of equations including M equations and N unknown parameters, and it can be expressed as:

$$\delta\phi = \mathrm{A}\phi \tag{8}$$

where each row of matrix $A[M\times N]$ corresponds to one interference pair, A[j, jSj]=1 and A[j, IMj]=-1, and the other elements are zero. A is a column full rank matrix when all interference pairs belong to the same baseline set. When $M = N$, the equation (8) have a unique solution. When $M > N$, the equations are an overdetermined equation, and the unique solution can be obtained under the constraints of the least squares.

$$\hat{\phi} = (\mathrm{A}^T A)^{-1}\mathrm{A}^T\delta\phi \tag{9}$$

When all interference pairs belong to different sets of baselines (assumed that there are L ($L > 1$) baselines sets), the rank of A is N-L+1 and rank is deficiency. Formula (9) A^TA is a singular matrix and there is no inverse matrix. Therefore, the singular value decomposition method is used to calculate the generalized inverse matrix A^+ of matrix A, and then to solve the least square minimum norm solution of equation (8). The calculation process can be referred to [20].

IV. EXPERIMENTAL ANALYSIS

A. Experimental data

The experimental data were obtained from ERS1/2 and ENVISAT-ASAR images. The ENVISAT-ASAR data were Track 176, frame 2997 and the ERS data were Track 405, Frame 2997. The scope was shown in Fig. 2. Considering Ms6.6 earthquake occurred in Dangxiong county (E:90.3, N:29.8) on October 6, 2008, large ground deformation occurred after the earthquake. Thus slow ground deformation before earthquake is analyzed in this paper. A total of 34 scenes of data before earthquake were selected from ENVISAT-ASAR data to study ground deformation. Data time was from April 6, 2003 to September 21, 2008. The data sets are shown in Table 1.

TABLE1 ENVISAT-ASAR data sets collected before Earthquake

Pair	Time (yyyymmdd)	Bperp（m）	Days	Pair	Time (yyyymmdd)	Bperp（m）	Days
1	20030406	-279.7	-980	18	20060430	338.5	140
2	20030511	438	-945	19	20060604	-643.5	175
3	20030615	-126.1	-910	20	20060709	1025.6	210
4	20030720	-245.9	-875	21	20060813	958.9	245
5	20030928	-318.4	-805	22	20061022	-361.2	315
6	20031102	-929	-770	23	20061126	-122.7	350
7	20031207	-264.2	-735	24	20061231	353.7	385
8	20040111	436.5	-700	25	20070311	416.3	455
9	20040215	-298.8	-665	26	20070415	-122.5	490
10	20040321	1030	-630	27	20070624	36.5	560
11	20040530	577.8	-560	28	20070729	-41.9	595
12	20041121	28.8	-385	29	20070902	220.7	630
13	20041226	15.4	-350	30	20071007	-133.7	665
14	20050724	568.8	-140	31	20071111	201.4	700
15	20050828	596.1	-105	32	20080504	-29.7	875
16	20051211	0	0	33	20080713	242	945
17	20060115	-812.3	35	34	20080921	-135.6	1015

Fig.2. SAR images covering study area (The left is ASAR 176-2997 and the right is ERS 405-2997)

B. *Experimental results*

SAR images collected in the experiment are original radar data. The data need to generate interferogram that can be processed by time series analysis. The main steps include the imaging of original data, registration of image, and the generation of interferogram.

(a) PS-InSAR time series analysis

PS-InSAR time series analysis mainly includes the selection of PS points, phase unwrapping, removal of orbit error, removal of terrain phase, estimation and removal of Dem error phase, and estimation and removal of atmospheric error phase. PS points were selected using the method proposed by Dr. Hooper.

When the PS points determined, the phase is unwrapped by Delaunay irregular triangle network method. According to formula (1), the phase values of each PS point include the phase of ground deformation, the phase of DEM error, the phase of atmospheric delay error and the phase of orbit error. In order to extract the phase value of ground deformation, other phase components should be estimated and eliminated. In order to eliminate the phase of atmospheric errors, Ferretti assumed that the phase of atmospheric error and the phase of orbital error were spatially related. In addition, high-pass filtering and low-pass filtering are performed on the unwrapping phase in time domain and space domain to estimate the phase of atmospheric error in each image. Phase of errors calculated from PS-InSAR method are shown in Fig. 3.

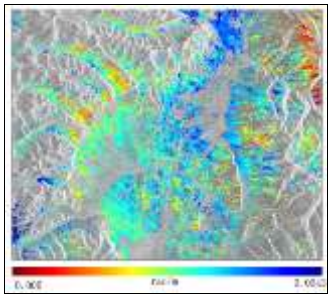

(a) DEM error phase

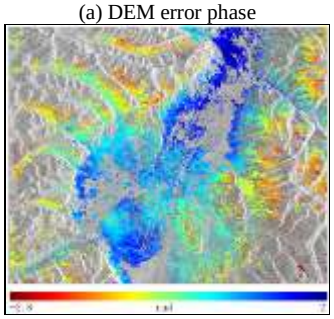

(b) Atmosphere and orbit error phase

Fig.3. Errors calculated from PS-InSAR method

(b) SBAS time series analysis

Different from PS time series analysis, the first step of SBAS time series analysis is to select the appropriate differential interference image pair. In experiment, 116 interference image pairs satisfying three conditions of spatial baseline less than 800m, time baseline less than 692 days, and the correlation coefficient greater than 0.65 were selected. The combination method is shown in Fig. 4. The 116 scenes interference image pair is registered using coherence coefficient method, and multiplied by multi-conjugate conjugate to obtain original interference images.

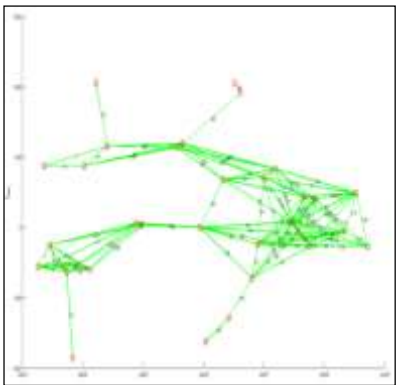

Fig.4. The combination method of interferograms

The stable phase points selected in SBAS time series analysis are called slowly-decorrelating filtered phase pixels (SDFP). After the SDFP point is determined, the same method as PS-InSAR is used to perform phase unwrapping to obtain the unwrapped differential phase. Based on formula (9), a matrix equation is established to obtain ground deformation amounts and deformation rates. The atmospheric phase window is also estimated and removed in the process of SBAS-InSAR processing. The method of estimating and removing the atmospheric phase window is the same as that used by PS-InSAR, namely high-pass filtering in time domain and low-pass filter in spatial domain. Phase of errors calculated from SBAS-InSAR method are shown in Fig. 5.

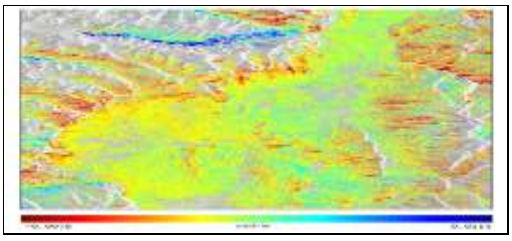

(a) DEM error phase

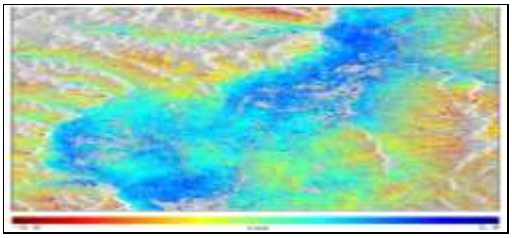

(b) Atmosphere and orbit error phase

Fig.5. Errors calculated from SBAS-InSAR method

After time series analysis and processing, the annual average radar in line of sight deformation rate field in the

study area is obtained. The standard variance of deformation rate in corresponding points is further calculated according to deformation sequence of all points, as shown in Fig. 6.

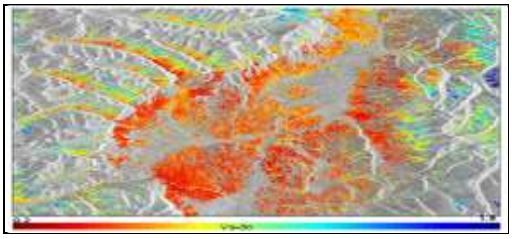

(a) Annual deformation rate obtained by PS-InSAR method

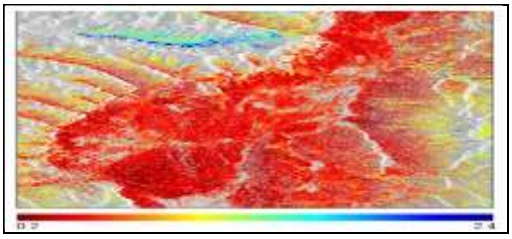

(b) Annual deformation rate obtained by SBAS-InSAR method

Fig.6. Standard variance of deformation rate

As can be seen from Fig. 6, most points have standard variance below 1.0 mm/yr, and only a few points have standard variance above 1.0 mm/yr. In order to improve the analysis accuracy, we set 1.0 mm/yr as the threshold. Unreliable points with standard variance above 1.0 mm/yr are removed. Filtered points are processed according to the PS-InSAR and SBAS-InSAR time series analysis methods respectively. Final deformation maps are obtained as shown in Fig. 7.

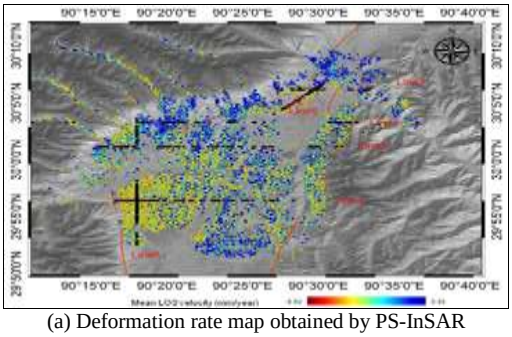

(a) Deformation rate map obtained by PS-InSAR

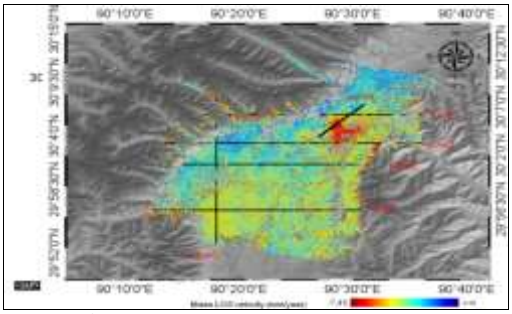

(b) Deformation rate map obtained by SBAS-InSAR

Fig.7. Deformation map of study area from 2003 to 2008

The average annual deformation rate map of the study area obtained by PS method is shown in Fig. 7(a). The average annual deformation rate of this area is -5.82~3.34 mm/yr. The average annual deformation rate map of the study area obtained by SBAS method is shown in Fig. 7 (b). The average annual deformation rate of this area is -7.45-4.99 mm/yr. Ground deformation obtained by these two methods is approximately the same.

C Results analysis

In order to visualize the overall deformation of the study area, six deformation rate profiles were made along both sides of Dangxiong-Yabajing basin, which were marked as line 1 - line 6. Location of each line is shown in Fig. 7. Deformation rates of these six profile lines are shown in Fig. 8.

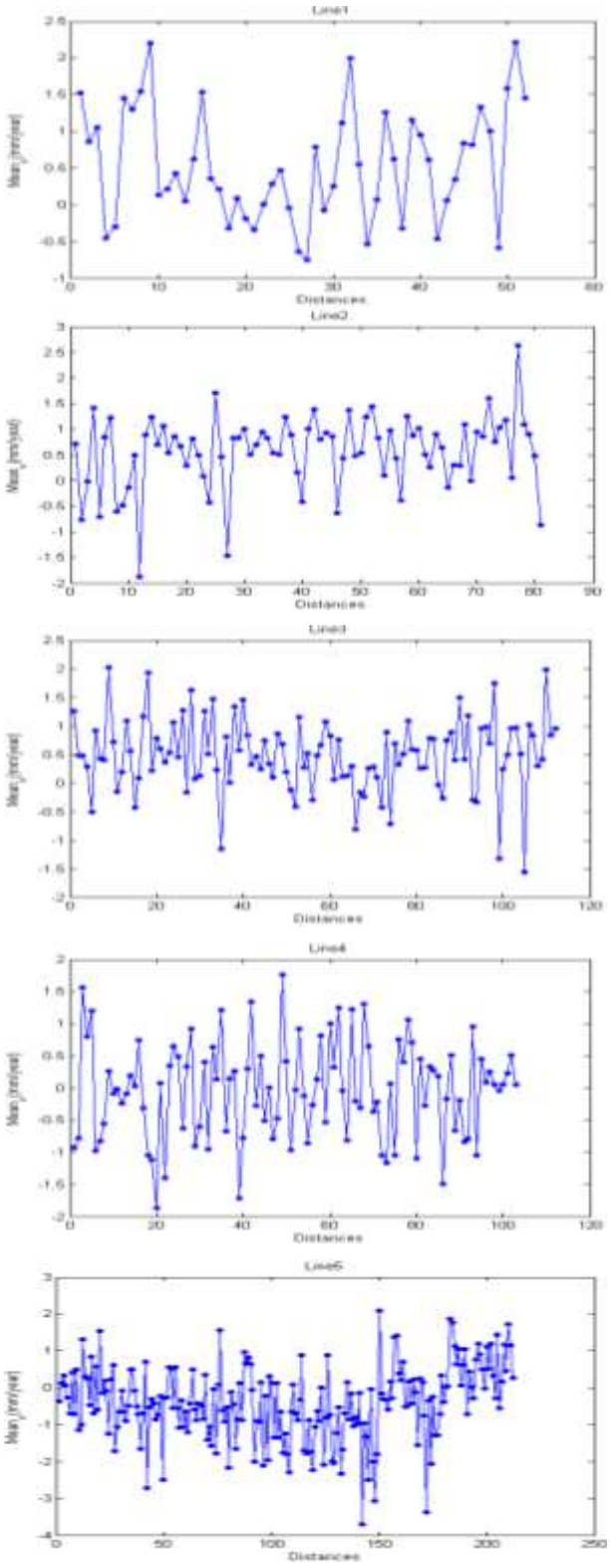

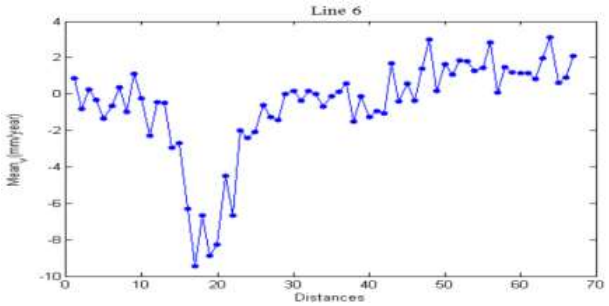

(a) Obtained by PS-InSAR

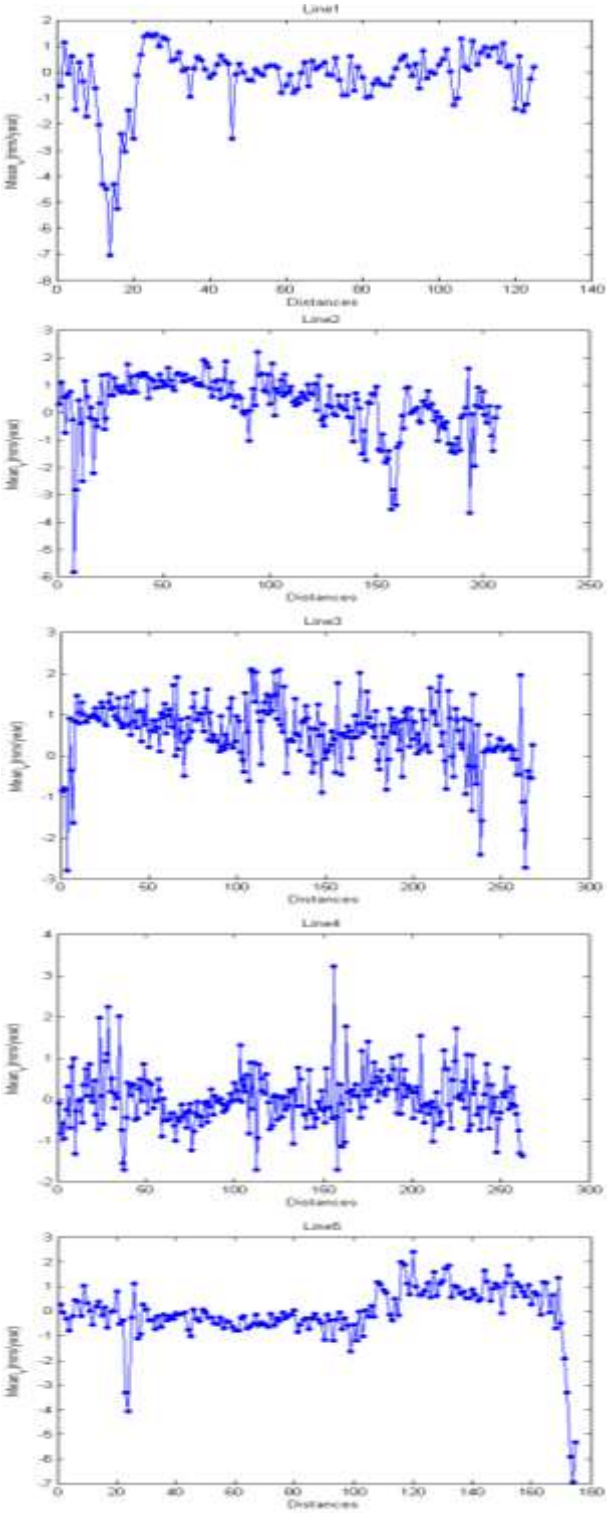

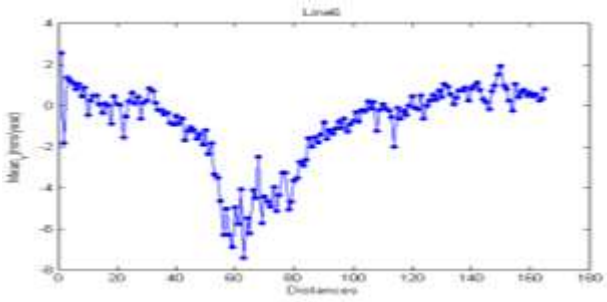

(b) Obtained by SBAS-InSAR

Fig.8. Curves of deformation rate of each profile

It can be seen that although the two methods are different in selecting stable points, calculating deformation and removing errors, the trends of deformation obtained is approximately the same. First, around the geothermal power station (line 1 and line 6), both methods gained large ground subsidence areas, and the maximum deformation rate was 5-8 mm/yr. This is due to the fact that this position is roughly located at the junction of southern fault of Nyenchen Tanglha (northwest margin of Yangbajing-Dangxiong basin) and the front fault of Tanggula Mountain (southeast margin of Yangbajing-Dangxiong basin). This position is rich in geothermal resources. Moreover, there are large thermal power stations, and the massive exploitation of geothermal resources leads to the large-scale ground subsidence in this area. Secondly, ignoring the ground subsidence caused by human factors (i.e. geothermal power station), trends of ground deformation obtained by these two methods is basically the same. Southern fault of Nyenchen Tanglha Mountain (northwest margin of Yangbajing-Dangxiong basin) presents a trend of ground uplift. Flat area in the middle of Yangbajing-Dangxiong basin presents a trend of ground subsidence. The front fault of Tanggula Mountain (southeast margin of Yangbajing-Dangxiong basin) presents a trend of ground subsidence. The reason for this phenomenon is that due to the fault activity, the high-level areas were pushed to uplift, while the low-lying areas were squeezed to subsidence. Monitoring results were accordance with fault movement in situ. This demonstrates that PS-InSAR and SBAS-InSAR are reliable in fault movement monitoring. Thus the fault activity can be analyzed based on monitoring results. This will provide data for earthquake prediction.

V. CONCLUSIONS

In this paper, 34 scenes ENVISAT-ASAR data covering Dangxiong area are processed by PS and SBAS time series analysis methods. These two results are basically consistent with each other. Combined with the geographical tectonics of Dangxiong area, it is determined that, due to the influence of fault movement, southern fault of Nyenchen Tanglha (northwest margin of Yangbajing-Dangxiong basin) presents a trend of ground uplift. Flat area in the middle of Yangbajing-Dangxiong basin presents a trend of ground subsidence. The front fault of Tanggula Mountain (southeast margin of Yangbajing-Dangxiong basin) presents a trend of ground subsidence. These results were accordance with fault movement in situ. When fault moving,

high-level areas were pushed to uplift, while the low-lying areas were squeezed to subsidence. This demonstrates that PS-InSAR and SBAS-InSAR are reliable in analyzing fault movement. Thus the fault activity can be analyzed based on PS-InSAR and SBAS-InSAR methods. This will provide data for earthquake prediction.

ACKNOWLEDGEMENT

This study was supported by the National Natural Science Foundation of China [grant numbers [51604164].

REFERENCES

[1] Zhang Jingfa, Gong Lixia, and Jiang Wenliang, “Application of PS InSAR technique to measurement of long-term crusta l deformation,” International seismic dynamics, vol. 6, pp. 1-6, 2006.

[2] Ramon F H. Subsidence monitoring using contiguous and PS-InSAR: Quality assessment based on precision and reliability. Proceedings, 11th FIG Symposium on Deformation Measurements, Santorini, Greece, 2003.

[3] Zebker H A, and Villasenor J, “Decorrelation in interferometric radar echoes,” IEEE Trans. Geosci. Remote Sensing, vol. 30, no. 5, pp. 950-959, 1992.

[4] Sang W K, Chang O K, and etc. Surface deformation in Mokpo area observed with synthetic aperture radar interferometry. Geoscience and Remote Sensing Symposium, IGARSS '05. Proceedings, IEEE International, Vol.1, pp. 3-5, 2005.

[5] Li Z H, Correction of atmospheric water vapour effects on Repeat-Pass SAR Interferometry Using GPS, MODIS and MERIS Data, London, Department of Geomatic Engineering, 2005.

[6] Chen Fulong, Zhang hong, and Wang Chao, “Automatic matching of Tie-points with high-resolution SAR images,” Journal of Image and Graphics, vol. 11, no. 09, pp. 1278-1281, 2006.

[7] Ferretti A, Rocca F, Prati C. Permanent scatterers in SAR interferometry, Proceeding of IGARSS, Hamburg, Germany, 28 June-2 July, 1999.

[8] Berardino P, Fornaro G, Lanari R, and et al. “A new algorithm for surface deformation monitoring based on small baseline differential SAR interferograms,” Geoscience and Remote Sensing, vol. 40, no. 11, pp. 2375-2383, 2002.

[9] Jo M J, Won J S, Kim S W, and et al. “A time-series SAR observation of surface deformation at the southern end of the San Andreas Fault Zone,” Geosciences Journal, vol. 14, no.3, pp. 277-287, 2010.

[10] Qu Chunyan, Shan Xinjian, and Song Xiaogang, “Preliminary study on crustal deformation of Haiyuan fault zone based on PS-InSAR technique,” Chinese Journal of Geophysics, vol. 54, no. 04, pp. 984-993, 2011.

[11] Meng Xiujun, Qu Chunyan, Shan Xinjian, and et al. “Application of PS-InSAR technique in monitoring crustal microdeformation in the northern margin of the western Qinling Mountains,” Seismology and Geology, vol. 36, no. 1, pp. 166-176, 2014.

[12] Fabio Canova, Cristiano Tolomei, Stefano Salvi, and et al. “Land subsidence along the Ionian coast of SE Sicily (Italy), detection and analysis via Small Baseline Subset (SBAS) multitemporal differential SAR interferometry,” Earth Surface Processes and Landforms, vol. 37, no. 3, pp. 273-286, 2012.

[13] Liu Zhimin, Li Yongsheng, Zhang Jingfa, and et al. “An analysis of surface deformation in the Changzhi mining area using small baseline InSAR,” Remot Sens Land Resour, vol. 26, no. 3, pp. 37-42, 2014.

[14] Sun Xiaopeng, Lu Xiaoya, Wen Xuehu, and et al. “Monitoring of ground subsidence in Chengdu Plain using SBAS－InSAR,” Remot Sens Land Resour, vol. 28, no. 3, pp. 123-129, 2016.

[15] Zhou Lv, Guo Jiming, Li Xin, and et al. “Monitoring and analyzing on ground settlement in Beijing area based on SBAS-InSAR,” Journal of Geodesy and Geodynamie, vol. 36, no. 9, pp. 793-797, 2016.

[16] Li ShanShan, Li Zhiwei, Hu Jun, and et al. “Investigation of the seasonal oscillation of the permafrost over Qinghai-Tibet plateau with SBAS-InSAR algorithm,” Chinese Journal of Geophysics, vol. 56, no.5, pp. 1476-1486, 2013.

[17] Dezheng Zhao, Chunyan Qu, Xinjian Shan, and et al. “InSAR and GPS derived coseismic eformation and fault model of the 2017 Ms7.0 Jiuzhaigou earthquake in the Northeast Bayanhar block,” Tectonophysics, vol. 726, no. 2018, pp. 86–99, 2018.

[18] Liu Yunhua, Zhang Guohong, Zhang Yingfeng, and et al. “Source parameters of the 2016 Menyuan earthquake in the northeastern Tibetan Plateau determined from regional seismic waveforms and InSAR measurements,” Journal of Asian Earth Sciences, vol. 158, pp. 103-111, 2018.

[19] Dehls J F, Basilico M, and Colesanti C. “Ground deformation monitoring in the Ranafjord area of Norway by means of the Pesistnet Scatterers technique. Geoscience & Remote Sensing Symposium,” IGARSS.2002 IEEE International, vol. 1, pp. 203-207, 2002.

[20] Berardino P, Fornaro G, Lanari R, and et al. “A new algorithm for surface deformation monitoring based on small baseline differential SAR interferograms,” Geoscience and Remote Sensing, vol. 40, no.11, pp. 2375-2383, 2002.